Theor Chem Acc (2016) 135:36
DOI 10.1007/s00214-015-1765-9

REGULAR ARTICLE

Thermal properties of the orthorhombic $CaSnO_3$ perovskite under pressure from ab initio quasi-harmonic calculations

J. Maul[1,2,3] · I. M. G. Santos[1] · J. R. Sambrano[2] · A. Erba[3]

Received: 24 September 2015 / Accepted: 16 November 2015 / Published online: 28 January 2016

Abstract Structural, elastic and thermodynamic properties of the orthorhombic $CaSnO_3$ perovskite are theoretically investigated at the ab initio level as a function of temperature and pressure. Harmonic and quasi-harmonic lattice dynamical calculations are performed with the CRYSTAL program, by explicitly accounting for thermal expansion effects and by exploring the effect of several DFT functionals. The anisotropic, directional elastic response of the system is characterized up to 20 GPa of pressure. The thermal lattice expansion and elastic bulk modulus are described at simultaneous temperatures up to 2000 K and pressures up to 20 GPa. The Gibbs free energy of formation of $CaSnO_3$ from CaO and SnO_2 as a function of temperature is also addressed by means of fully converged phonon dispersion calculations on the three systems.

Keywords Quasi-harmonic · CaSnO · Perovskite · Pressure–temperature · CRYSTAL program

Published as part of the special collection of articles "CHITEL 2015 - Torino - Italy".

✉ J. Maul
jmaul@quimica.ufpb.br

[1] Laboratório de Combustíveis e Materiais, INCTMN-UFPB, Universidade Federal da Paraíba, João Pessoa, PB CEP 58051-900, Brazil

[2] Grupo de Modelagem e Simulação Molecular, INCTMN-UNESP, São Paulo State University, Bauru, SP CEP 17033-360, Brazil

[3] Dipartimento di Chimica, Università di Torino and NIS, Nanostructured Interfaces and Surfaces, Centre of Excellence, Via Giuria 5, 10125 Turin, Italy

1 Introduction

Perovskites of the ABO_3 family are receiving special attention in recent years due to their peculiar physical and chemical properties, which lead to many possible applications [1–8]. Calcium stannate, $CaSnO_3$, is known as an effective phosphorous host [9–20], for its potential as constituent of multifunctional optoelectronic devices [21], and for its unconventional luminescent behavior [22–24]. At ambient conditions, $CaSnO_3$ exhibits a orthorhombic $GdFeO_3$-type perovskite structure belonging to the *Pbnm* space group, which is expected to be stable up to pressures of about 40 GPa and temperatures of about 2000 K [25]. Other phases have been reported (ilmenite-like, hexagonal, rhombohedral, tetragonal and cubic) [26–29], the orthorhombic one remaining the most studied [30–38]. Many fundamental properties of this material, however, still have to be reliably determined, which is the case of its thermal properties (its thermal structural and elastic features, its thermodynamic behavior, etc.). Furthermore, the evolution under increasing pressure of such thermal response properties is still not known, which would be of geochemical interest as $CaSnO_3$ is structurally and chemically closely related to $CaSiO_3$ and $MgSiO_3$ (two common constituents of the Earth mantle) [33, 39–41]. In a recent study, we have investigated the effect of pressure on some vibrational spectroscopic features (Raman and IR spectra) of $CaSnO_3$ by means of ab initio calculations [42].

In the present study, a series of state-of-the-art ab initio techniques is used for the inclusion of temperature and pressure effects on several properties (structural, elastic, thermodynamic) of the orthorhombic phase of the $CaSnO_3$ perovskite. A recently developed fully automated scheme, as implemented in a development version of the CRYSTAL14

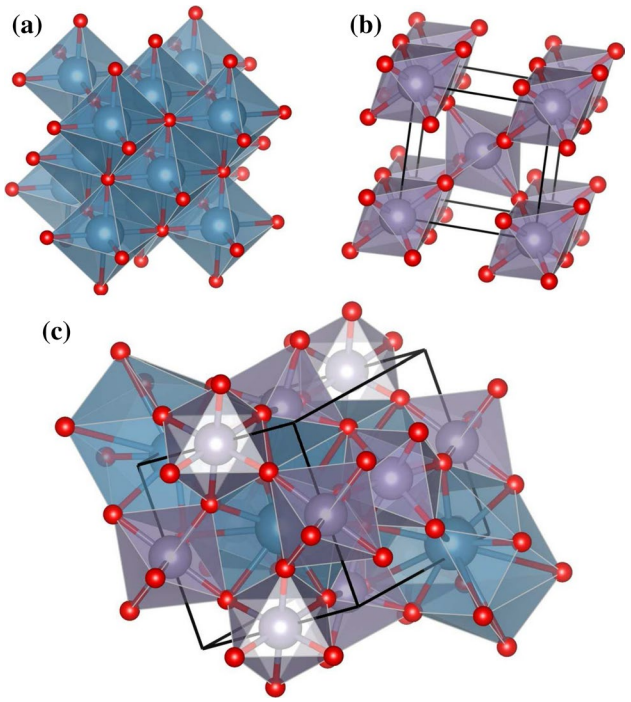

Fig. 1 (color online) Structure of **a** cubic CaO ($Fm\bar{3}m$), **b** tetragonal SnO_2 ($P4_2/mnm$) and **c** orthorhombic $CaSnO_3$ ($Pbnm$) [59]

program [43], is used for performing quasi-harmonic calculations [44, 45], which allows to go beyond the standard harmonic approximation to the lattice potential and to effectively compute the directional thermal lattice expansion, temperature dependence of the bulk modulus, difference between constant-pressure and constant-volume specific heats, adiabatic bulk modulus, etc. [46–50]. In this respect, it is worth mentioning that a recent experimental study by Redfern et al. [51] suggested $CaSnO_3$ to be highly quasi-harmonic (without the need for an explicit anharmonic description of the system, then). The anisotropic elastic response of the system (in terms of elastic constants and directional seismic wave velocities) is investigated as a function of pressure [52–56]. Furthermore, the full phonon dispersion of the system is computed, which allows us to investigate other thermodynamic properties of the system and phonon density-of-states [57, 58]. The Gibbs free energy of formation of $CaSnO_3$ from the two simple oxides CaO (cubic) and SnO_2 (tetragonal) is also evaluated as a function of temperature. The atomic structure of the three crystals is sketched in Fig. 1.

The effect of the exchange-correlation functional of the density functional theory (DFT) on different properties (structural, thermal, elastic) is documented by considering different levels of approximation: from local-density, to generalized-gradient, to hybrids and range-separated hybrids.

2 Computational methodology and setup

All calculations are performed using a development version of the CRYSTAL14 program [43]. An all-electron atom-centered Gaussian-type-function (GTF) basis set is adopted, where Ca, Sn and O atoms are described by 8(s)6511(sp)21(d), 9(s)763111(sp)631(d) and 6(s)2111(sp)1(d) contractions of primitive GTFs, respectively [42]. Seven different DFT functionals are adopted: SVWN [60, 61], PBE [62], PBEsol [63], B3LYP [64, 65], PBE0 [66], HSE06 [67] and HISS [68, 69].

The tolerances for the evaluation of Coulomb and exchange infinite series are set to default values for all calculations. The shrinking factor is set to 8, which corresponds to a sampling over 125 independent **k**-points within the first Brillouin zone in reciprocal space. The convergence on energy of the SCF procedure is set to the tight value of 10^{-10} hartree.

Phonon dispersion calculations are performed with supercells (SC) of different sizes within the PBE level of theory. For CaO, two SCs of 216 and 512 atoms are used, for SnO_2, two SCs containing 384 and 750 atoms and for $CaSnO_3$, SCs with 160 and 540 atoms. Quasi-harmonic calculations on CaO and SnO_2 have been performed with SCs of 54 and 48 atoms, respectively.

2.1 Quasi-harmonic properties

A fully automated scheme for computing quasi-harmonic properties of crystals has recently been implemented in the CRYSTAL program, which relies on computing and fitting (with a cubic polynomial function) harmonic vibration frequencies at different volumes after having performed volume-constrained geometry optimizations [46–50]. Harmonic phonon frequencies are computed by diagonalizing the dynamical matrix following a "direct space" approach [46, 57, 70, 71]. Constant-volume specific heat, $C_V(T)$, and entropy, $S(T)$, are estimated through standard statistical thermodynamics from harmonic phonon frequencies as computed at the equilibrium zero-temperature, zero-pressure volume. Quasi-harmonic properties are computed by considering a volume range extending from a $-3\,\%$ compression to a $+6\,\%$ expansion with respect to the equilibrium volume; four equidistant volumes are considered in this interval.

The *isotropic* thermal expansion coefficient, $\alpha_V(T)$, of the system is obtained by minimizing the isothermal Helmholtz free energy

$$F^{\mathrm{QHA}}(T,V) = U_0^{\mathrm{ZP}}(V) + k_{\mathrm{B}}T \sum_{\mathbf{k}p} \left[\ln\left(1 - e^{-\frac{\hbar\omega_{\mathbf{k}p}(V)}{k_B T}}\right)\right] \quad (1)$$

with respect to volume at several temperatures, where k_B is Boltzmann's constant and $U_0^{ZP}(V)$ is the zero-temperature internal energy of the crystal which includes the zero-point energy of the system: $E_0^{ZP}(V) = \sum_{\mathbf{k}p} \hbar\omega_{\mathbf{k}p}(V)/2$. The *anisotropic* thermal expansion can be computed as well [48].

The quasi-harmonic approximation (QHA) allows for combining pressure and temperature effects on structural and elastic properties of materials. By differentiating Eq. (1) with respect to the volume and changing sign, the thermal pressure is obtained:

$$P(V;T) = -\frac{\partial F^{\mathrm{QHA}}(V;T)}{\partial V}. \tag{2}$$

The description of the isothermal bulk modulus of the system at simultaneous high temperatures and high pressures, $K_T(P,T)$, can be obtained as an isothermal second derivative of Eq. (1) with respect to the volume and by exploiting relation (2):

$$K_T(P,T) = V(P,T)\left(\frac{\partial^2 F^{\mathrm{QHA}}(V(P,T);T)}{\partial V(P,T)^2}\right)_T. \tag{3}$$

2.2 Pressure-constrained structure optimization

A fully analytical scheme, based on the stress tensor, is used for optimizing the crystal volume under a given external pressure [72]. The stress tensor $\boldsymbol{\sigma}$ is a symmetric second-rank tensor that can be computed in terms of analytical energy gradients with respect to lattice parameters:

$$\sigma_{ij} = \frac{1}{V}\frac{\partial E}{\partial \epsilon_{ij}} = \frac{1}{V}\sum_{k=1}^{3}\frac{\partial E}{\partial a'_{ki}}a_{kj}, \tag{4}$$

with $\boldsymbol{\epsilon}$ second-rank symmetric pure strain tensor and $i,j,k = x,y,z$. In the expression above, a_{ij} are elements of a 3×3 matrix, $\mathbf{A}$, where Cartesian components of the three lattice vectors $\mathbf{a}_1$, $\mathbf{a}_2$ and $\mathbf{a}_3$ are inserted by rows and V is the cell volume. When a distortion is applied to the cell, the lattice parameters transform as $a'_{ij} = \sum_{k=1}^{3}(\delta_{jk} + \epsilon_{jk})a_{ik}$, where δ_{jk} is the Kronecker delta. By adding an external hydrostatic "prestress" $\sigma_{ij}^{\mathrm{pre}} = P\delta_{ij}$ to σ_{ij} and by inverting Eq. (4), one gets the expression for the constrained gradients

$$\frac{\partial H}{\partial a_{ij}} = \frac{\partial E}{\partial a_{ij}} + PV(\mathbf{A}^{-1})_{ji}. \tag{5}$$

With the inclusion of a hydrostatic pressure, the function to be minimized becomes the enthalpy $H = E + PV$ [73].

2.3 Elastic tensor calculation

If any finite prestress is absent, second-order elastic constants are simply defined as second energy density derivatives with respect to pairs of infinitesimal Eulerian strains:

$$C_{ijkl} = \frac{1}{V_0}\left(\frac{\partial^2 E}{\partial \epsilon_{ij}\partial \epsilon_{kl}}\right)_{\epsilon=0}. \tag{6}$$

An automated scheme for the calculation of the elastic tensor has been implemented in the CRYSTAL program [52, 74] that has been generalized also to low-dimensionality 1D and 2D systems [75]. Applications of this scheme cover a wide range of materials [76–84].

When a finite prestress $\boldsymbol{\sigma}^{\mathrm{pre}}$ is applied in the form of a hydrostatic pressure P, within the frame of finite Eulerian strain, the elastic stiffness constants become [85–89]:

$$B_{ijkl} = C_{ijkl} + \frac{P}{2}(2\delta_{ij}\delta_{kl} - \delta_{il}\delta_{jk} - \delta_{ik}\delta_{jl}), \tag{7}$$

provided that the volume V_0 at which Eq. (6) is evaluated is replaced by the equilibrium volume $V(P)$ at pressure P. A fully automated implementation in the CRYSTAL program of the calculation of the stiffness tensor $\mathbf{B}$ (and of $\mathbf{S} = \mathbf{B}^{-1}$, the compliance tensor) under pressure has recently been presented [53, 54]. A two-index representation of the elastic stiffness tensor is obtained ($B_{ijkl} \rightarrow B_{vu}$) by exploiting Voigt's notation, according to which $v,u = 1,\ldots,6\,(1 = xx, 2 = yy, 3 = zz, 4 = yz, 5 = xz, 6 = xy)$ [90]. For the elastic constant calculation, four strained configurations are considered for each independent strain, with a dimensionless strain amplitude of 0.0075 (i.e., 0.75 %).

3 Results and discussion

3.1 Quasi-harmonic description

The thermal expansion of $CaSnO_3$ as theoretically determined by means of quasi-harmonic lattice dynamical calculations is reported in Fig. 2. The lower panel of the figure reports the equilibrium cell volume as a function of temperature, up to 1000 K, as obtained with seven different DFT functionals and as compared to available experimental data (empty symbols) [51, 91]. We can clearly see that while different functionals provide rather different descriptions of the absolute value of the equilibrium volume, they all describe a similar trend as it comes to the temperature dependence. As expected, the LDA functional underestimates the cell volume. Two functionals (the generalized-gradient PBE and the global hybrid B3LYP) significantly overestimate the volume, while the other functionals provide a reasonable description of the equilibrium structure. The two experimental datasets reported in the figure show some large discrepancies between each other as regards the lattice expansion. Data by Chen et al. [91], which measure

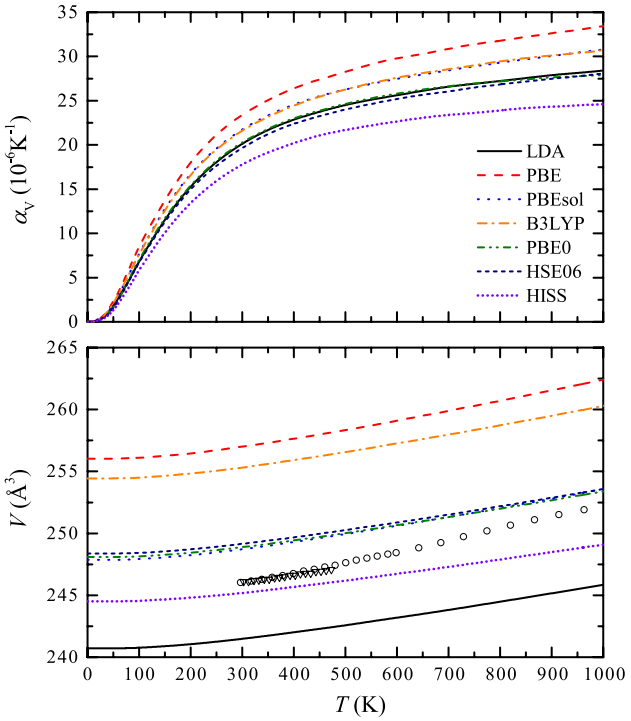

Fig. 2 (color online) Thermal expansion coefficient (*upper panel*) and temperature-dependent cell volume (*lower panel*) of $CaSnO_3$ up to 1000 K, as computed with seven different DFT functionals. *Empty circles* and *triangles* are experimental data from Redfern et al. [51] and from Chen et al. [91], respectively

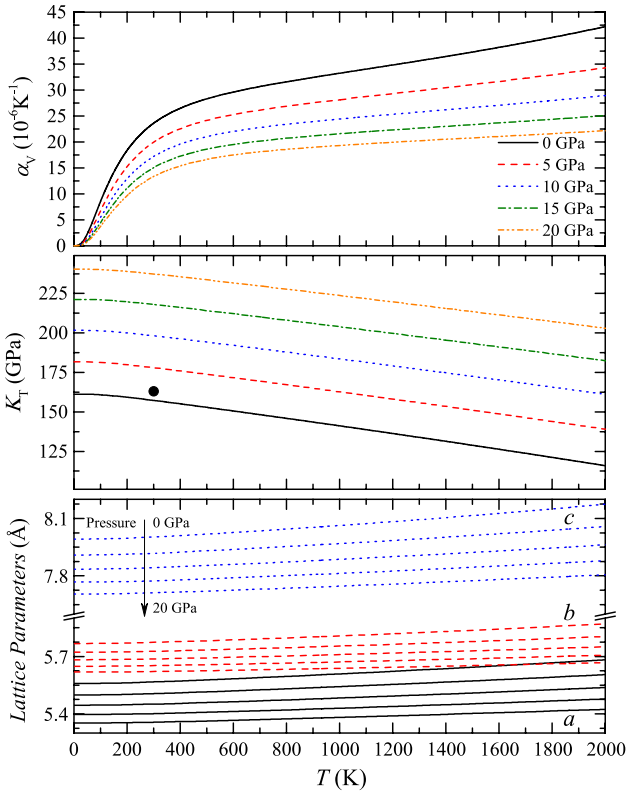

Fig. 3 (color online) Thermal expansion coefficient (*upper panel*), isothermal bulk modulus (*middle panel*) and lattice parameters (*lower panel*) of $CaSnO_3$ as a function of temperature, at 5 different pressures from 0 to 20 GPa. In the middle panel, the *full circle* represents the experimental value for the isothermal bulk modulus at room conditions [33]. All data are obtained with the PBE functional

a lower expansion, are found to better agree with present quasi-harmonic simulations than those by Redfern et al. [51], where a much larger thermal expansion is reported.

In order to better highlight the different description of thermal expansion given by different functionals, we may refer to the upper panel of Fig. 2, where the volumetric thermal expansion coefficient $\alpha_V(T) = 1/V(T)[\partial V(T)/\partial T]$ is reported. Although all functionals provide a similar description of the lattice thermal expansion of $CaSnO_3$, some fine differences can be noticed: The HISS functional shows the smallest thermal expansion, while the PBE one the largest (followed by PBEsol and B3LYP, which give an almost identical description of α_V). The other three adopted functionals provide a rather similar description with each other.

The quasi-harmonic approximation represents an effective theoretical tool for describing structural and average elastic properties of solids at simultaneous high pressure and high temperature that is at extreme conditions which are difficult to be explored experimentally. In Fig. 3, we report the thermal evolution, up to 2000 K, of the thermal expansion coefficient, of the isothermal bulk modulus and of the three independent lattice parameters a, b and c, at five different pressures up to 20 GPa, as obtained with the PBE functional. From a computational point of view, the lattice dynamics of the system has been evaluated at 15 volumes from a $-10\,\%$ compression to a 10 % expansion of the equilibrium zero-pressure, zero-temperature volume. From the upper panel of the figure, we can see that the thermal expansion coefficient behaves quite regularly up to 2000 K (with a tiny deviation from linearity), thus confirming the high quasi-harmonic character of $CaSnO_3$. As pressure increases, the thermal expansion obviously decreases and the coefficient becomes even more regular and linear at high temperatures, as expected given that pressure tends to suppress explicit anharmonic terms in the lattice potential. The evolution of the isothermal bulk modulus as a function of pressure and temperature is quantitatively given in the middle panel of the figure, where the experimental value at room conditions is also given as a full circle [33]. In the lower panel of the figure, the directional, anisotropic, thermal expansion of orthorhombic $CaSnO_3$ is documented. The a and c lattice parameters are found to expand more than the b one by about a factor of 1.2.

Experimentally, a much larger factor of about 4.3 was suggested by Redfern et al. [51], which seems way too large for a system such as $CaSnO_3$, which is not very structurally anisotropic. This large experimental anisotropy of the thermal expansion is reflected in the large volumetric thermal expansion reported in Fig. 2 (see empty circles).

3.2 Phonon dispersion and thermodynamics

Thermodynamic properties require a good description of phonon dispersion in order to be accurately described at the ab initio level. In this section, we report converged harmonic (constant-volume specific heat C_V and entropy S_V) and quasi-harmonic (constant-pressure specific heat C_P and entropy S_P) thermodynamic properties of $CaSnO_3$. Furthermore, thermodynamic functions of both CaO and SnO_2 are studied, with the purpose in mind to determine the formation free energy of the following solid-state reaction [28, 94]:

$$CaO_{(s)} + SnO2_{(s)} \rightarrow CaSnO3_{(s)} \tag{8}$$

These thermodynamic functions are reported in Fig. 4 for the three systems up to 2000 K of temperature. Harmonic properties are obtained with the largest super-cells considered (see Sect. 2 for details), which ensure full convergence as regards the sampling of phonon dispersion within the Brillouin zone. The quasi-harmonic constant-pressure specific heat is obtained by summing on top of the harmonic C_V, the term $C_P(T) - C_V(T) = \alpha_V^2(T)K_T(T)V(T)T$, as derived from the quasi-harmonic quantities given in Figs. 2 and 3. Experimental data from Gurevich et al. [92] (full circles) and from Robie [93] (empty circles) are also reported, when available. We can see that our calculations provide a satisfactory description of the entropy (a key ingredient to the study of the formation free energy), apart from a slight underestimation at very high temperatures. Specific heat of CaO is also reasonably described, whereas for SnO_2 we get a poor description of the constant-pressure specific heat, due to a large underestimation of the thermal expansion (the quasi-harmonic approximation seems to fail rather dramatically for this system). Absolute values of C_V and C_P at room temperature (in units of J/mol K) are: 40.77 and 41.18 for CaO; 55.92 and 56.06 for SnO_2 and 98.24 and 99.26 for $CaSnO_3$, respectively.

The formation Gibbs's free energy of the solid-state reaction (8) is given in Table 1 at few different temperatures. The $CaSnO_3$ perovskite is found to be thermodynamically more stable than the two isolated oxides at all temperatures, which is consistent with the experimentally observed "irreversibility" of $CaSnO_3$ once formed from both oxides or molten salts [16, 28, 34, 94–97].

From the full phonon dispersion of a system, the phonon density-of-state (PDOS) can be determined, which is defined by Eq. [58]:

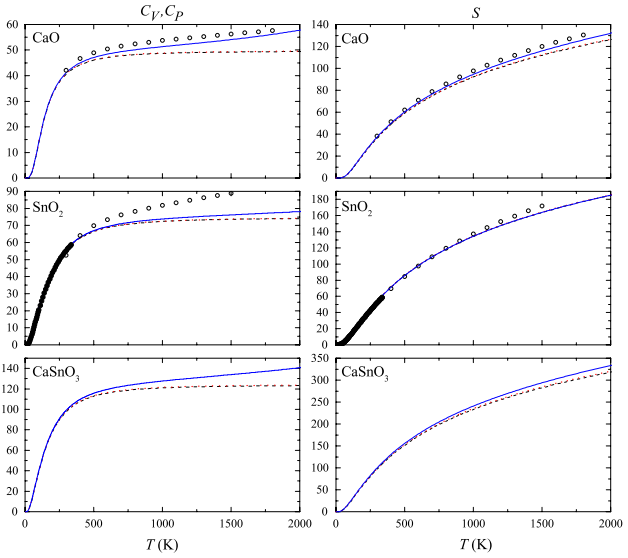

Fig. 4 (color online) Heat capacity (*left panel*) and entropy (*right panel*) of $CaSnO_3$, CaO and SnO_2. All data in J mol^{-1}K^{-1}. In the left panels, *dashed* and *dotted lines* refer to C_V and *continuous lines* to C_P, in the *right ones*, to S_V and S_P, respectively. *Full circles* are experimental data by Gurevich et al. [92] while *empty ones* by Robie [93]

$$g(\omega) = \frac{1}{V_{\mathrm{BZ}}} \int_{\mathrm{BZ}} \sum_{p=1}^{3N} \delta(\omega_{\mathbf{k}p} - \omega) d\mathbf{k} \,, \tag{9}$$

where V_{BZ} is the volume of the Brillouin zone and the integration is performed over it. From Eq. (9), it is seen that the PDOS is normalized to $3N$, being N the number of atoms per cell ($\int g(\omega)d\omega = 3N$). The total PDOS can be partitioned into atomic contributions $g(\omega) = \sum_a g_a(\omega)x_a$ where the sum runs over the atomic species of the system, x_a is the fraction of atomic species a, and

$$g_a(\omega) = \frac{1}{n_{\mathbf{k}}} \sum_{p,\mathbf{k}} |\mathbf{e}_{p,\mathbf{k};a}|^2 \delta(\omega_{\mathbf{k}p} - \omega) \,, \tag{10}$$

where $\mathbf{e}_{p,\mathbf{k}}$ are the eigenvectors of the dynamical matrices $W^{\mathbf{k}}$ and the integral in Eq. (9) has been replaced by the sum over the $n_{\mathbf{k}}$ sampled $\mathbf{k}$-points within the first Brillouin zone. Atomic PDOSs are useful tools for discussing which atoms are mostly involved in phonons of given spectral regions. Figure 5 reports the total PDOS (black continuous line) as well as the atomic PDOSs of Ca, Sn and the two symmetry-independent oxygen atoms, apical O_{ap} and equatorial O_{eq}. The PDOS of $CaSnO_3$ clearly shows three distinct regions: a broad one ranging from 0 up to about 440 cm^{-1}, a second one from about 450 to about 625 cm^{-1} and a third sharp one at about 700 cm^{-1}. The optical vibrational spectrum above approximatively 350 cm^{-1} is almost entirely dominated by motions of the oxygen atoms (see yellow and green lines).

Table 1 Gibbs free energy of formation of $CaSnO_3$ from the CaO and SnO_2 oxides, as determined with the PBE functional

T (K)	ΔG (kJ/mol)
0	−58.65
300	−59.98
1000	−65.32
2000	−73.19

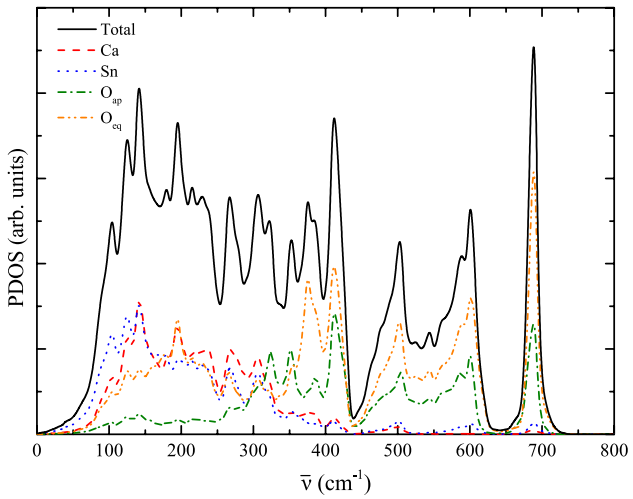

Fig. 5 (color online) Total and atomic phonon density-of-states of $CaSnO_3$

At lower wave-numbers, all atoms are involved in the lattice vibrations, Ca and Sn atoms becoming dominant in very soft collective phonon modes.

3.3 Elastic properties

This section is devoted to the discussion of the anisotropic elastic response of $CaSnO_3$, at ambient conditions and under pressure. The fourth-rank elastic tensor of the orthorhombic $CaSnO_3$ perovskite has 9 symmetry-independent elastic constants C_{vu}, which are reported in Table 2 as computed with several DFT functionals. All functionals describe similarly the anisotropy of the elastic response, given that the ratios among the elastic constants are similar in all cases. On the contrary, absolute values differ rather significantly. Single-crystal elastic constants of $CaSnO_3$ have not yet been experimentally measured so that the performance of the different functionals can be evaluated just on average elastic properties. Following the Voigt-Reuss-Hill (VRH) averaging scheme [98], average elastic properties of isotropic polycrystalline aggregates can be derived starting from computed elastic constants. The average bulk modulus $\overline{K}$ obtained in this way is given in the table. Computed elastic properties refer to 0 K and neglect even zero-point motion effects. From the quasi-harmonic calculations discussed before, however, the isothermal bulk modulus K_T can be computed as a function of temperature. Some experimental techniques for measuring the bulk modulus of a crystal involve elastic waves and are characterized by very short timescales that prevent the system from reaching a thermal equilibrium; in these cases, an adiabatic bulk modulus, K_S, is measured instead. Adiabatic and isothermal bulk moduli do coincide with each other at zero temperature only, K_S always being larger than K_T at any finite temperature. The quasi-harmonic approximation also offers a way to compute the adiabatic bulk modulus from the isothermal one, given that:

Table 2 Single-crystal elastic constants C_{vu} $CaSnO_3$ as computed with seven DFT functionals at 0 K

	LDA	PBE	PBEsol	B3LYP	PBE0	HSE06	HISS	Exp. [33]
C_{11}	284.6	260.9	269.1	288.2	295.9	293.7	318.3	
C_{22}	351.1	299.5	328.0	325.0	343.8	341.2	366.6	
C_{33}	317.0	281.1	300.0	305.9	324.0	320.6	349.1	
C_{44}	100.1	90.5	95.8	99.3	104.6	104.0	112.9	
C_{55}	77.8	74.3	76.1	83.9	86.8	86.1	94.4	
C_{66}	103.0	90.6	97.7	97.7	105.9	105.1	114.2	
C_{12}	150.7	124.6	136.0	127.9	138.7	139.9	147.2	
C_{13}	121.2	100.6	110.9	107.3	114.3	113.1	121.0	
C_{23}	120.7	100.7	108.9	106.3	111.8	113.0	118.4	
$\overline{K}$	192.3	165.6	178.1	177.7	187.8	187.1	200.5	
K_S^{300}	185.6	159.4	172.1	171.0	180.4	180.6	194.9	167.2
K_T^{300}	183.9	157.7	170.4	169.3	178.7	179.0	193.4	162.6

The VRH average bulk modulus $\overline{K}$ at 0 K and the isothermal K_T and adiabatic K_S bulk moduli at 300 K of temperature are also reported. All data in GPa

Table 3 Elastic stiffness constants B_{vu} (in GPa) of $CaSnO_3$ under pressure up to 20 GPa, as computed with the PBE functional

Pressure	0 GPa	5 GPa	10 GPa	15 GPa	20 GPa
B_{11}	260.9	276.1	292.2	308.9	322.3
B_{22}	299.5	335.1	363.0	390.7	418.2
B_{33}	281.1	308.6	332.6	356.2	380.2
B_{44}	90.5	96.4	101.5	105.6	109.8
B_{55}	74.3	77.4	79.9	81.8	83.7
B_{66}	90.6	98.0	103.4	108.5	114.2
B_{12}	124.6	143.4	166.0	185.8	206.8
B_{13}	100.6	118.3	134.5	150.4	165.8
B_{23}	100.7	115.9	133.1	148.2	163.4
$\overline{K}$	165.6	185.5	205.2	223.8	242.1
$\overline{G}$	85.0	89.8	92.9	96.0	98.8
$\overline{E}$	217.7	231.9	242.1	251.9	260.9
σ	0.281	0.292	0.303	0.312	0.320
$\overline{v}_p$	7.181	7.407	7.594	7.764	7.924
$\overline{v}_s$	3.960	4.015	4.040	4.063	4.087

Average elastic properties are also reported such as bulk modulus $\overline{K}$, shear modulus $\overline{G}$, Young modulus $\overline{E}$ (in GPa), Poisson's ratio σ (dimensionless) and longitudinal $\overline{v}_p$ and transverse $\overline{v}_s$ seismic wave velocities (in km/s)

$$K_S = K_T + \frac{\alpha_V^2 V T K_T^2}{C_V} = K_T \times \frac{C_P}{C_V}, \tag{11}$$

where the dependence of all quantities on temperature is just omitted for clarity sake. In Table 2, both the isothermal and adiabatic bulk moduli are reported at room temperature and compared with available experimental data. From that comparison, we see that the HISS functional provides the most rigid description of the system, followed by LDA and both PBE0 and HSE06. On the other hand, PBE, PBEsol and B3LYP provide a softer description of the system, which is seen to be much closer to the experimental elastic rigidity of $CaSnO_3$.

The effect of an applied hydrostatic pressure on the elastic properties of $CaSnO_3$ is documented in Table 3, where elastic stiffness constants B_{vu} (computed as described in Sect. 2.3) are reported along with other average elastic properties, such as the average bulk $\overline{K}$ and shear $\overline{G}$ moduli obtained within the VRH scheme. From the bulk modulus and the average shear modulus, Young's modulus $\overline{E}$ and Poisson's ratio σ can be defined as well:

$$\overline{E} = \frac{9\overline{K}\overline{G}}{3\overline{K} + \overline{G}} \quad \text{and} \quad \sigma = \frac{3\overline{K} - 2\overline{G}}{2(3\overline{K} + \overline{G})}. \tag{12}$$

Average values of transverse (shear) and longitudinal seismic wave velocities, for an isotropic polycrystalline aggregate, can also be computed from the elastic constants and the density ρ of the crystal as:

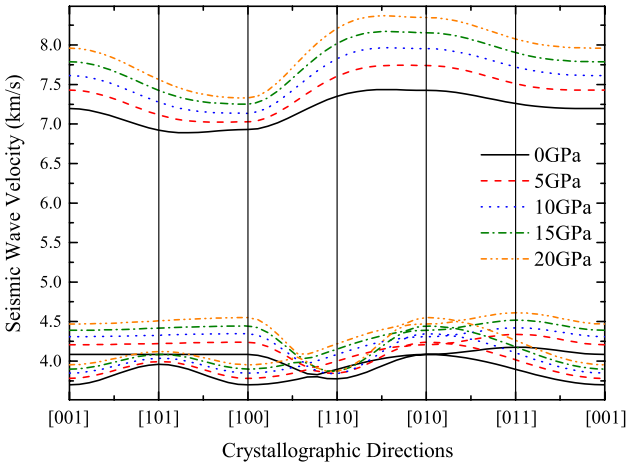

Fig. 6 (color online) Directional seismic wave velocities of $CaSnO_3$ under pressures up to 20 GPa, as computed with the PBE functional

$$\overline{v}_s = \sqrt{\frac{\overline{G}}{\rho}} \quad \text{and} \quad \overline{v}_p = \sqrt{\frac{\overline{K} + 4/3\overline{G}}{\rho}}. \tag{13}$$

As expected, all elastic constants do increase as pressure increases. The diagonal elastic constants B_{22} and B_{33} are the ones that increase faster with pressure with slopes of 5.9 and 4.9, respectively, followed by B_{12} with a slope of 4.1. Shear constants display a small dependence on pressure, B_{55} being the less affected by pressure with a slope of just 0.5. Transverse seismic wave velocities are not much affected by pressure (with a derivative of 0.006 km/s/GPa), at variance with longitudinal ones (with 0.037 km/s/GPa); these values are in qualitative agreement with experimental determinations by Schneider et al. [99] of 0.012 and 0.052 km/s/GPa, respectively.

The propagation of elastic waves in a crystal is an anisotropic physical phenomenon, which, once the fourth-rank elastic tensor has been determined, can be fully characterized by solving Christoffel's Eq. [100, 101]. Directional seismic wave velocities (a quasi-longitudinal v_p one and two quasi-transverse v_{s1} and v_{s2} ones) of $CaSnO_3$, as computed at different pressures in the present study, are reported in Fig. 6. It is seen that the directions of minimum propagation velocity of longitudinal waves are between the [101] and [001] ones, whereas along directions from [110] and [010] longitudinal waves propagate with the largest velocity. Apart from an obvious increase in the average propagation velocity, the effect of pressure on the anisotropic propagation of elastic waves in calcium stannate is found to be relatively small, with just a slight increase in the anisotropy of longitudinal waves.

4 Conclusions

State-of-the-art techniques for the ab initio investigation of solids have been applied to predict structural, elastic and thermodynamic properties of the orthorhombic $CaSnO_3$ perovskite at high temperatures and pressures, which are not yet experimentally known. Harmonic and quasi-harmonic calculations, as combined with advanced algorithms for the calculation of anisotropic elastic properties, do indeed constitute a powerful tool for the quantum-chemical description of solids at *P* and *T* conditions of real interest in fields such as material science and geochemistry.

The effect on computed properties of the DFT functional is explicitly discussed. Functionals belonging to four families of the DFT (local-density, generalized-gradient, hybrid and range-separated hybrid approximations) are considered. If large differences on absolute values of computed properties are found, most properties are seen to be almost independent of the adopted functional as regards their behavior as a function of temperature or pressure. The generalized-gradient PBE and PBEsol and the global hybrid B3LYP functionals are found to provide the best description of the elastic features of the system.

Acknowledgments J.M. acknowledges the Brazilian scholarship program "Ciência sem Fronteiras" (Process Number 248425/2013-7/SWE). Furthermore, we are grateful for the programs PROCAD 2013/Proc. 88881.068492/2014-01 and FAPESP (2013/19289-0, 2013/07296-2) and also to the Center for Scientific Computing of the São Paulo State University (GridUNESP).

References

1. Peña MA, Fierro JLG (2001) Chem Rev 101(7):1981
2. Royer S, Duprez D, Can F, Courtois X, Batiot-Dupeyrat C, Laassiri S, Alamdari H (2014) Chem Rev 114(20):10292
3. Kubacka A, Fernández-García M, Colón G (2012) Chem Rev 112(3):1555
4. Thalinger R, Opitz AK, Kogler S, Heggen M, Stroppa D, Schmidmair D, Tappert R, Fleig J, Klötzer B, Penner S (2015) J Phys Chem C 119(21):11739
5. An L, Onishi H (2015) ACS Catal 5(6):3196
6. Armstrong EN, Duncan KL, Wachsman ED (2013) Phys Chem Chem Phys 15:2298
7. Yang Y, Íñiguez J, Mao AJ, Bellaiche L (2014) Phys Rev Lett 112:057202
8. Misono M (2013) In: Misono M (ed) Heterogeneous catalysis of mixed oxides perovskite and heteropoly catalysts, studies in surface science and catalysis, vol 176. Elsevier, Amsterdam, pp 67–95
9. Liu Z, Liu Y (2005) Mater Chem Phys 93(1):129
10. Lei B, Li B, Zhang H, Li W (2007) Opt Mater 29(11):1491
11. Lei B, Li B, Zhang H, Zhang L, Cong Y, Li W (2007) J Electrochem Soc 154(7):H623
12. Fu Z, Li W, Du S, Yang HK, Jeong JH (2009) J Electrochem Soc 156(10):J308
13. Ueda K, Shimizu Y (2010) Thin Solid Films 518(11):3063
14. Chen XY, Ma C, Bao SP, Zhang HY (2010) J Alloys Compd 497(1–2):354
15. Pang XL, Jia CH, Li GQ, Zhang WF (2011) Opt Mater 34(1):234
16. Nakamura T, Shima M, Yasukawa M, Ueda K (2012) J Sol-Gel Sci Technol 61(2):362
17. Liang Z, Zhang J, Sun J, Li X, Cheng L, Zhong H, Fu S, Tian Y, Chen B (2013) Phys B 412:36
18. Zhang J, Chen B, Liang Z, Li X, Sun J, Cheng L, Zhong H (2014) J Alloys Compd 612:204
19. Kim SD, Hwang KS, Hwangbo S (2013) Electron Mater Lett 9(4):405
20. Hwang KS, Jeoni YS, Hwangbo S, Kim JT (2013) Ceram Int 39(7):8555
21. Ueda K, Maeda T, Nakayashiki K, Goto K, Nakachi Y, Takashima H, Nomura K, Kajihara K, Hosono H (2008) Appl Phys Express 1(1):015003
22. Karabulut Y, Ayvacıklı M, Canimoglu A, Garcia Guinea J, Kotan Z, Ekdal E, Akyuz O, Can N (2014) Spectrosc Lett 47(8):630
23. Orsi Gordo V, Tuncer Arslanli Y, Canimoglu A, Ayvacikli M, Galvão Gobato Y, Henini M, Can N (2015) Appl Radiat Isotopes 99(0):69
24. Canimoglu A, Garcia-Guinea J, Karabulut Y, Ayvacikli M, Jorge A, Can N (2015) Appl Radiat Isotopes 99:138
25. Tateno S, Hirose K, Sata N, Ohishi Y (2010) Phys Earth Planet Inter 181(1–2):54
26. Durand B, Loiseleur H (1978) J Appl Crystallogr 11(4):289
27. Ropp R (2013) In: Ropp R (ed) Encyclopedia of the alkaline earth compounds. Elsevier, Amsterdam, pp 351–480
28. Coffeen WW (1953) J Am Ceram Soc 36(7):207
29. Hautier G, Miglio A, Waroquiers D, Rignanese GM, Gonze X (2014) Chem Mater 26(19):5447
30. Mizoguchi H, Eng HW, Woodward PM (2004) Inorg Chem 43(5):1667
31. Tarrida M, Larguem H, Madon M (2009) Phys Chem Miner 36(7):403
32. Yangthaisong A (2013) Chin Phys Lett 30(7):077101
33. Kung J, Angel RJ, Ross NL (2001) Phys Chem Miner 28(1):35
34. Kung J, Lin YJ, Lin CM (2011) J Chem Phys 135(22):224507
35. McMillan P, Ross N (1988) Phys Chem Miner 16(1):21
36. Vegas A, Vallet-Regí M, González-Calbet JM, Alario-Franco MA (1986) Acta Crystallogr Sect B Struct Sci 42(2):167
37. Cherrad D, Maouche D, Boudissa M, Reffas L, Louail M, Maamache M, Haddadi K, Medkour Y (2013) Phys B 429:95
38. Moreira E, Barboza CA, Albuquerque EL, Fulco UL, Henriques JM, Araiújo AI (2015) J Phys Chem Solids 77:85
39. Caracas R, Cohen RE (2005) Geophys Res Lett 32(6):L06303
40. Kuskov O, Galimzyanov R (1986) In: Saxena S (ed) Chemistry and physics of terrestrial planets advances in physical geochemistry, vol 6. Springer, New York, pp 310–361
41. Liebermann RC, Jones LEA, Ringwood AE (1977) Phys Earth Planet Inter 14(2):165
42. Maul J, Erba A, Santos IMG, Sambrano JR, Dovesi R (2015) J Chem Phys 142(1):014505
43. Dovesi R, Orlando R, Erba A, Zicovich-Wilson CM, Civalleri B, Casassa S, Maschio L, Ferrabone M, De La Pierre M, D'Arco Ph, Noël Y, Causá M, Rérat M, Kirtman B (2014) Int J Quantum Chem 114:1287
44. Allen RE, De Wette FW (1969) Phys Rev 179:873
45. Boyer LL (1979) Phys Rev Lett 42:584
46. Erba A (2014) J Chem Phys 141:124115
47. Erba A, Shahrokhi M, Moradian R, Dovesi R (2015) J Chem Phys 142:044114
48. Erba A, Maul J, Demichelis R, Dovesi R (2015) Phys Chem Chem Phys 17:11670

49. Erba A, Maul J, De La Pierre M, Dovesi R (2015) J Chem Phys 142:204502
50. Erba A, Maul J, Itou M, Dovesi R, Sakurai Y (2015) Phys Rev Lett 115:117402
51. Redfern SAT, Chen C, Kung J, Chaix-Pluchery O, Kreisel J, Salje EKH (2011) J Phys Condens Matter 23(42):425401
52. Erba A, Mahmoud A, Orlando R, Dovesi R (2014) Phys Chem Miner 41:151
53. Erba A, Mahmoud A, Belmonte D, Dovesi R (2014) J Chem Phys 140:124703
54. Mahmoud A, Erba A, Doll K, Dovesi R (2014) J Chem Phys 140:234703
55. Lacivita V, Erba A, Dovesi R, D'Arco Ph (2014) Phys Chem Chem Phys 16:15331
56. Erba A, Navarrete-López AM, Lacivita V, D'Arco P, Zicovich-Wilson CM (2015) Phys Chem Chem Phys 17:2660
57. Erba A, Ferrabone M, Orlando R, Dovesi R (2013) J Comput Chem 34:346
58. Baima J, Ferrabone M, Orlando R, Erba A, Dovesi R (2015) Phys Chem Minerals. doi:10.1007/s00269-015-0781-6
59. Momma K, Izumi F (2011) J Appl Crystallogr 44(6):1272
60. Dirac PAM (1930) Proc Cambridge Phil Soc 26:376
61. Vosko SH, Wilk L, Nusair M (1980) Can J Phys 58:1200
62. Perdew JP, Burke K, Ernzerhof M (1996) Phys Rev Lett 77:3865
63. Perdew JP, Ruzsinszky A, Csonka GI, Vydrov OA, Scuseria GE, Constantin LA, Zhou X, Burke K (2008) Phys Rev Lett 100:136406
64. Becke AD (1993) J Chem Phys 98:5648
65. Lee C, Yang W, Parr RG (1988) Phys Rev B 37:785
66. Adamo C, Barone V (1999) J Chem Phys 110:6158
67. Krukau AV, Vydrov OA, Izmaylov AF, Scuseria GE (2006) J Chem Phys 125(22):224106
68. Henderson TM, Izmaylov AF, Scuseria GE, Savin A (2007) J Chem Phys 127(22):221103
69. Henderson TM, Izmaylov AF, Scuseria GE, Savin A (2008) J Chem Theory Comput 4(8):1254
70. Parlinski K, Li ZQ, Kawazoe Y (1997) Phys Rev Lett 78:4063
71. Togo A, Oba F, Tanaka I (2008) Phys Rev B 78:134106
72. Doll K (2010) Mol Phys 108(3–4):223
73. Souza I, Martins J (1997) Phys Rev B 55:8733
74. Perger WF, Criswell J, Civalleri B, Dovesi R (2009) Comput Phys Commun 180:1753
75. Erba A, Ferrabone M, Baima J, Orlando R, Rérat M, Dovesi R (2013) J Chem Phys 138:054906
76. Erba A, El-Kelany KE, Ferrero M, Baraille I, Rérat M (2013) Phys Rev B 88:035102
77. Mahmoud A, Erba A, El-Kelany KE, Rérat M, Orlando R (2014) Phys Rev B 89:045103
78. Erba A, Dovesi R (2013) Phys Rev B 88:045121
79. El-Kelany KE, Erba A, Carbonnière P, Rérat M (2014) J Phys Cond Matter 26:205401
80. Baima J, Erba A, Orlando R, Rérat M, Dovesi R (2013) J Phys Chem C 117:12864
81. Lacivita V, Erba A, Noël Y, Orlando R, D'Arco Ph, Dovesi R (2013) J Chem Phys 138:214706
82. Tan JC, Civalleri B, Erba A, Albanese E (2015) CrystEngComm 17:375
83. El-Kelany KE, Carbonnière P, Erba A, Rérat M (2015) J Phys Chem C 119:8966
84. Erba A, Ruggiero MT, Korter TM, Dovesi R (2015) J Chem Phys 143:144504
85. Karki BB, Ackland GJ, Crain J (1997) J Phys Cond Matter 9(41):8579
86. Wang J, Li J, Yip S, Phillpot S, Wolf D (1995) Phys Rev B 52:12627
87. Karki BB, Stixrude L, Wentzcovitch RM (2001) Rev Geophys 39:507
88. Wallace DC (1972) Thermodynamics of crystals. Wiley, New York
89. Wallace DC (1965) Rev Mod Phys 37:57
90. Nye JF (1957) Physical properties of crystals. Oxford University Press, Oxford
91. Chen CJ, Kung J, Lin CM, Zhang M (2010) S.A.T. Redfern, ArXiv e-prints
92. Gurevich VM, Gavrichev KS, Polyakov VB, Clayton RN, Mineev SD, Hu G, Gorbunov VE, Golushina LN (2004) Thermochim Acta 421(1–2):179
93. Robie RA, Hemingway BS, Fisher JR (1978) Thermodynamic properties of minerals and related substances at 298.15 k and 1 bar (105 pascals) pressure and at higher temperatures. Tech Rep B 1452, United States Geological Survey
94. Tanaka Y (1942) Bull Chem Soc Jpn 17(2):70
95. Lu Z, Liu J, Tang Y, Li Y (2004) Inorg Chem Commun 7(6):731
96. Zhao J, Ross NL, Angel RJ (2004) Phys Chem Miner 31(5):299
97. Shojaei S, Hassanzadeh-Tabrizi SA, Ghashang M (2014) Ceram Int 40(7(Part A)):9609
98. Hill R (1963) J Mech Phys Solids 11:357
99. Schneider BW, Liu W, Li B (2008) High Pressure Res 28(3):397
100. Musgrave MJP (1970) Crystal acoustics. Holden-Day, San Francisco
101. Auld BA (1973) Acoustic fields and waves in solids. Krieger Publishing Company, Malabar